J Mater Sci: Mater Electron (2022) 33:22835–22850

Effect of Bi_2O_3 on structural and optical properties of $Li_2O{\cdot}PbO{\cdot}Bi_2O_3{\cdot}B_2O_3$ glasses

Sumit Chauhan[1,2], Rajni Bala[1,*], Sanjay Gaur[3], and Saroj Rani[4]

[1] Department of Physics, Maharshi Dayanand University, Rohtak, Haryana 124001, India
[2] Department of Physics, Government College for Women, Bawani Khera, Haryana 127032, India
[3] Department of Physics, GDC Memorial College, Bahal (Bhiwani), Haryana 127028, India
[4] Department of Physics, Government P. G. College, Panchkula, Haryana 134109, India

Received: 3 July 2022
Accepted: 3 September 2022
Published online: 28 September 2022

ABSTRACT

The quaternary glass system has a composition of $30Li_2O{\cdot}20PbO{\cdot}xBi_2O_3{\cdot}(50\text{-}x)B_2O_3$ (where x = 0, 10, 20, 30, and 40 mol%) was fabricated by using the melt quench technique at the temperature 1100 °C. The broad haloes obtained by the XRD diffractograms confirm the amorphous nature of the samples. Density, molar volume, and crystalline volume were found to be increased depending on Bi_2O_3 concentration. Structural properties were studied with the help of FTIR spectroscopy in the range of 400–2000 cm^{-1}. The analysis of IR spectra reveals the presence of octahedral [BiO_6], [BO_4], [PbO_4], and tetrahedral [BiO_3], [BO_3] structural units in the present glasses. Increases in bismuth concentration result in the transformation of [BO_3] structural units to [BO_4] structural units. The presence of a sharp cutoff and broad transmission region make these glasses suitable for spectral devices. The cutoff wavelength, optical band gap, and Urbach's energy were estimated using UV absorption spectra. The increase in cutoff wavelength and decrease in band gap with bismuth content can be associated with the rise in non-bridging oxygens. Urbach's energy values revealed that the defect concentration could be controlled by the presence of Bi_2O_3 content in the present glass system. The values of optical parameters, viz., refractive index, molar refractivity, molar polarizability, electronic polarizability, optical basicity, and theoretical optical basicity, increase with Bi_2O_3 content. The high values of refractive index and low metallization criterion indicate that the studied glass system may be potentially used for non-linear optical applications.

Address correspondence to E-mail: khattak.rajni@gmail.com

https://doi.org/10.1007/s10854-022-09050-7

1 Introduction

Many researchers have found that heavy metal oxide glasses (HMOGs) containing basic glass former, such as B_2O_3 have applications in photonics and optoelectronics, such as optical lenses, colored TV tubes, and optical limiters, and can be used as laser materials, etc. [1–3]. Borate is one of the best glass former and flux materials used in all heavy metal oxide glasses because of its small cation size (B^{3+}) and high bond strength [2]. Due to its high chemical durability and thermal stability, it can form glass easily at low temperatures [3–5]. It exhibits high photonic properties, i.e., good clearness, optimal bandwidths, better-infrared transmissions, and high mechanical stability [6]. The boron atom is commonly coordinated with three or four oxygen atoms and produces [BO_3] or [BO_4] structural units in borate glasses. These two fundamental parts can merge in any way and are also called superstructure [7, 8]. Each alkali oxide is related to a proportionate quantity of B_2O_3 in alkali borate glass systems. Therefore, the number of structural units is determined by the total concentration of additional modifiers [9, 10]. Lead oxide (PbO) plays a dual role of modifier and former. When Pb–O exhibits covalent bonds, they are used in IR transmitting devices, ultra-low loss waveguides, and optical grating. When PbO_4 is mixed with bismuth borate glasses, it shows better stability in oxide glasses. Glasses made of lead borate oxide are transparent in the visible and near-infrared ranges and have excellent glass formation properties over a wide compositional range. Optical and electrical devices, thermal and mechanical sensors, and reflecting windows are the applications of PbO-containing glasses [11]. Lithium borate glasses systems have been intensively researched because of their significant role in solid electrolytes for thin-film batteries. The ionic radius of lithium ion is ≈0.76 Å [12]. The small atomic number, isotropic ion conductivity, lightweight, and highly electro-positive character of lithium ions make it possible to use it in high voltage and high energy density microbatteries [13]. Bismuth occurs in a monoclinic form and has an ionic radius of octahedral adjustment of six oxygen atoms, and they are placed at a distance from 2.14 to 2.29 Å, wherein three oxygen atoms are much closer, approximately 2.29 Å [14]. Bismuth ions exist in Bi^{+}, Bi^{3+}, Bi^{4+}, and Bi^{5+} states. Bi^{3+} cation is more stable than other Bi cations and contributes more toward highly non-linear optical susceptibility [15, 16]. Borate glasses show different structural units, such as metaborate, di borate, pentaborate, orthoborate, and pyroborate [17–19]. Various properties of borate glasses with different constituents in ternary system Bi_2O_3–B_2O_3 [18], PbO-Bi_2O_3-B_2O_3 [17], ZnO–Bi_2O_3–B_2O_3 [3, 20], BaO–Bi_2O_3–B_2O_3 [20], PbO–Li_2O–B_2O_3 [21], PbF_2·Bi_2O_3·B_2O_3 [22], Li_2O–MgO–Bi_2O_3–B_2O_3 [7], and Li_2O·Bi_2O_3·WO_3·B_2O_3 [23] are studied by many researchers. M. Subhadra et al. [24] reported the impact of V_2O_5 content on the optical and physical characteristics of lithium bismuth borate glasses. Their investigations revealed that the density, molar volume, and optical basicity of these glasses increase, whereas interionic separation, polaron radius, glass transition temperature, and bandgap energy decrease due to increasing concentrations NBOs with the addition of V_2O_5. Study of lithium zinc bismuth borate glasses revealed that Bi^{3+} cations are incorporated in the glass network as [BiO_6] octahedral units at lower Bi_2O_3 content while it enters in the glass matrix both as [BiO_6] octahedral units and [BiO_3] pyramidal units at higher concentration. The variation in physical properties and structural changes occurring in the glasses was also correlated with the Bi_2O_3:B_2O_3 ratio [25]. E. M. Abou Hussein et al. prepared quaternary lithium bismuth silicate glass system with, PbO, BaO, or SrO and revealed that Pb^{2+} ions play an effective role in enhancing the electrical and optical properties of glass due to highly compact structure, low concentration of NBOs, defects or vacancies, and high polarizability [26]. Bhemarajan et al. [27] have presented a comparative study on bismuth borate lithium glasses with different modifier oxides and demonstrate the suitability of the glasses for various photonic applications. A number of researchers have worked to accurately incorporate the heavy metal oxide in the matrix of the glasses to improve their physical characteristics as radiation shielding materials [28–30]. Additionally, to the best of our knowledge, there are only a limited number of thorough and exhaustive researches on the structural and optical studies of heavy metal oxide containing lithium borate glasses in the literature. In our previous work, we have prepared Li_2O·PbO·Bi_2O_3·SiO_2 glasses [31] with varying concentrations of Bi_2O_3 (0–50 mol%). The physical, structural, and optical features of such glasses were also evaluated. The authors conclude that the density of glasses is

enhanced with increasing Bi_2O_3 content. FTIR structural analysis revealed the presence of Bi_2O_3 as network former with BiO_3 and as modifier with BiO_6 units.

The present study aims to prepare a new glass system having composition $30Li_2O.20PbO.xBi_2O_3.(50\text{-}x)B_2O_3$ (where x = 0–40 mol%) and investigate the influence of bismuth on the physical and structural characteristics of the prepared glass system. The above glasses have still not been synthesized to our knowledge, and also the FTIR and optical parameters have not been published to date. In addition, the optical properties of these glasses have been correlated with structural features by calculating the various optical parameters.

2 Experimental details

Glass samples having composition $30Li_2O{\cdot}20PbO{\cdot}xBi_2O_3{\cdot}(50\text{-}x)B_2O_3$ (x ranging from 0 to 40 in steps of 10) were taken. Different compositions with codes

B0: $30Li_2O{\cdot}20PbO{\cdot}50B_2O_3$
B1: $30Li_2O{\cdot}20PbO{\cdot}10Bi_2O_3{\cdot}40B_2O_3$
B2: $30Li_2O{\cdot}20PbO{\cdot}20Bi_2O_3{\cdot}30B_2O_3$
B3: $30Li_2O{\cdot}20PbO{\cdot}30Bi_2O_3{\cdot}20B_2O_3$
B4: $30Li_2O{\cdot}20PbO{\cdot}40Bi_2O_3{\cdot}10B_2O_3$

were prepared by using AR grade chemicals (99.5%) purity. First, the appropriate amounts of these chemicals lithium carbonate (Li_2CO_3), lead oxide (PbO), bismuth oxide (Bi_2O_3), and boric acid (H_3BO_3) are mixed in an agate pestle mortar. Then the mixture was put in a porcelain crucible and heat it in a programmable electric muffle furnace at a temperature of 1100 °C, maintained for half an hour. After that mixture is placed onto a stainless-steel plate, and another plate is pressed immediately at room temperature. To confirm the amorphous nature of the prepared samples, X-ray patterns of the glass samples have been recorded by using a Rigaku Table-Top X-ray diffractometer with source Cu K_α radiation in the 2θ range 10°–80° at a scanning rate of 10°/min. The density (D) of glass samples has been measured using the weight displacement method (Archimedes principle), using xylene as an immersion fluid. The glass transition temperature (T_g) was measured using Differential Scanning Calorimeter (Model Mettler Toledo Q20) maintained at a temperature of 10 °C/min. FTIR spectra were recorded using a Perkin Elmer Spectrum BX II spectrophotometer in the range of 400–4000 cm^{-1} using powder samples mixed with KBr in the ratio of 1:20 in reference materials. The optical absorption spectra of glass samples were recorded using UV–Vis-NIR spectrophotometer model Shimadzu (UV 3600 plus) in the range of 190–3300 nm. Different types of fitting, like multiple peak fitting, linear, and non-linear fitting, have been fitted using origin pro 8.8 software.

3 Results and discussion

3.1 X-ray diffraction and physical properties

XRD results of the present glasses show the absence of any sharp peaks depicted in Fig. 1. The presence of broad haloes ~ 28° confirmed the lack of long-range order and ascertained the amorphous nature of the glass samples.

Density is a very useful parameter to investigate the degree of structure compactness, changes or modification in the coordination or geometrical configurations, and variation of the dimensions of the glass network. Also, how tightly atomic groups and atoms in a glass network are placed together is mainly related to molar volume and density. The

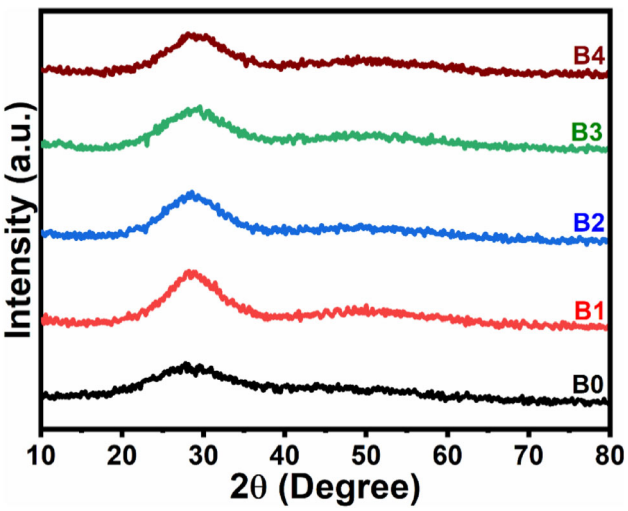

Fig. 1 X-ray diffractogram for all the compositions of $30Li_2O{\cdot}20PbO{\cdot}xBi_2O_3{\cdot}(50\text{-}x)B_2O_3$ glasses

density of each glass sample was determined using the Archimedes principle according to the formula,

$$D = \left(\frac{W_a}{W_a - W_x}\right) \times D_{xy}, \quad (1)$$

where W_a is the weight of the sample in air and W_x is the weight of the sample in xylene respectively, and D_{xy} is the density of xylene (= 0.8645 g/cm^3). The measured values of density for all the samples (B0 to B4) are presented in Table 1 and variation with Bi_2O_3 concentration is shown in Fig. 2a. It is found that the density of glass samples increases from 3.63 to 4.96 g/cm^3 with Bi_2O_3 content, which is ascribed to a lower molecular mass of B_2O_3 (69.62a.m.u) systematically replaced by a higher molecule mass of Bi_2O_3 (465.98a.m.u). Similar, trends in density values were also observed by Kaur et al. [32] in bismuth-containing lithium borate glasses and by Rani et al. [25] in $30Li_2O{\cdot}20ZnO{\cdot}xBi_2O_3{\cdot}(50\text{-}x)B_2O_3$ glass system. It helps us to determine the compactness of the glass network. The molar volume (V_m) and crystalline volume (V_C) are calculated by the following relations [33]:

$$V_m = \sum \frac{x_i M_i}{D}, \quad (2a)$$

where x_i and M_i are the molar fraction and molecular mass of the *i*th content.

$$V_C = x_i V_i, \quad (2b)$$

where V_i is the molar volume of an *i*th component in the crystalline phase. The values of molar volume for the crystalline phase were taken as Li_2O (14.84 cm^3), PbO (23.42 cm^3), Bi_2O_3 (52.36 cm^3), and B_2O_3 (27.30 cm^3). Figure 2b shows the molar and crystalline volume increases with bismuth content, and their values are demonstrated in Table.1. It is also clear from Table 1 that not much change in V_m and V_C values are observed for $x \leq 10$ afterward, there is a significant difference in V_m and V_C, which indicates excess structural volume increases with bismuth content. This is due to the increase of non-bridging oxygen ions in the glass matrix at the expense of Bi_2O_3 content. Further, It is concluded that bismuth ions have a large ionic radius than other constituents; expanding the glass structure and therefore, the molar volume of glass increases.

DSC thermograms of the synthesized glasses are presented in Fig. 3a. These thermograms provide the value of glass transition temperature as listed in Table 1, with the endotherm representing the rigidity and strength of the glass. Figure 3b reveals the compositional dependence of T_g. From the figure, it is observed that when the concentration of bismuth oxide is increased up to 20 mol%, the value of T_g increased and after that decreased (above 20 mol%). The decreasing behavior of these glass samples suggests the modifying role of bismuth oxide on the glass matrix. This result is supported by IR studies. As the borate oxide is replaced by bismuth oxide, $[BO_3]$ structural units are transformed into $[BO_4]$ structural units due to which the concentration of non-bridging oxygens increases in the glass matrix.

The oxygen molar volume (V_o) represented in Eq. (3) is defined as the volume of glass carrying one mole of oxygen and is determined by the molar volume [27]:

$$V_o = \frac{V_m}{\sum_i x_i n_i}, \quad (3)$$

In which x_i is the molar fraction and n_i represents the number of oxygen atoms in each oxide, respectively. Using the standard formula in Eq. (4), the oxygen

Table 1 Density (D), molar volume (V_m), crystalline volume (V_C), glass transition temperature (T_g), oxygen molar volume (V_o), oxygen packing density (OPD), ionic concentration (N), polaron radius (r_p), inter ionic distance (r_i), field strength (F), fraction of BO_4 units (N_4) of $30Li_2O{\cdot}20PbO{\cdot}xBi_2O_3{\cdot}(50\text{-}x)B_2O_3$ glasses

Parameter	B0	B1	B2	B3	B4
D (g/cm^3)	3.63	4.29	4.46	4.59	4.96
V_m(cm^3/mol)	24.35	29.84	37.59	45.16	49.78
V_C (cm^3/mol)	22.78	25.29	27.79	29.38	32.81
T_g (°C)	353.83	402.67	428.06	398.76	382.09
V_o (cm^3/mol)	12.17	14.92	18.79	22.58	24.89
OPD (mol/l)	82.14	67.02	53.20	44.28	40.17
$N \times 10^{21}$(ions/cm^3)	–	2.02	3.20	3.99	4.84
$r_p \times 10^{-8}$(cm^{-1})	–	3.19	2.73	2.54	2.38
$r_i \times 10^{-8}$(cm^{-1})	–	7.91	6.79	6.30	5.91
$F \times 10^{15}$ (cm^{-2})	–	2.95	4.03	4.65	5.30
N_4	0.365	0.089	0.106	0.109	0.094

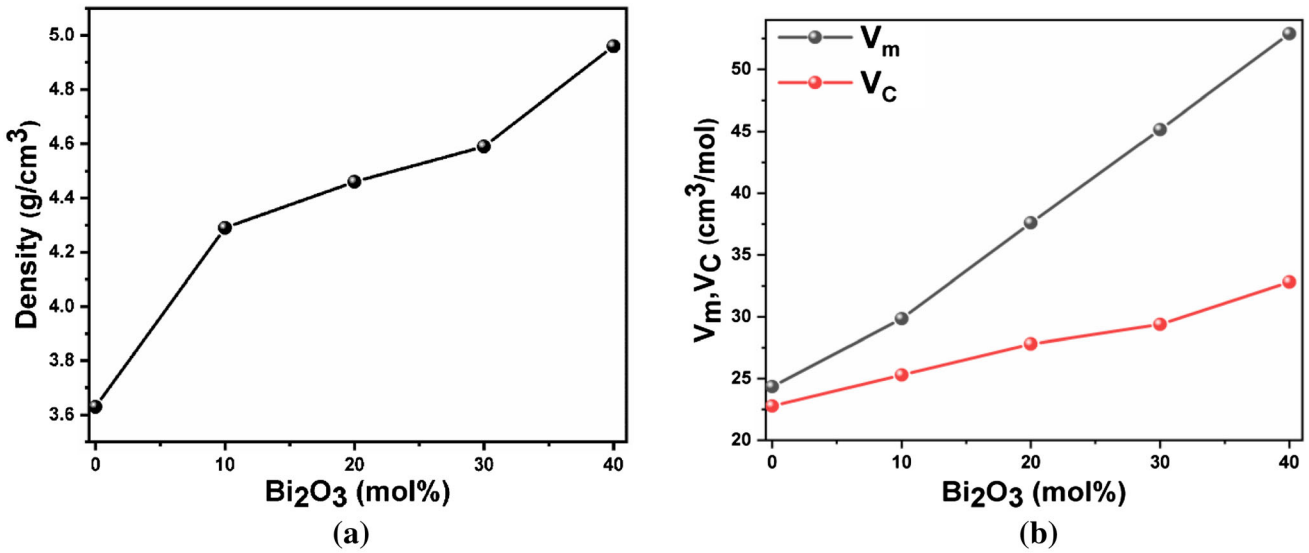

Fig. 2 **a** Compositional variation of density for all the compositions of $30Li_2O{\cdot}20PbO{\cdot}xBi_2O_3{\cdot}(50\text{-}x)B_2O_3$ glasses. **b** Compositional variation of V_C and V_m with bismuth content for $30Li_2O{\cdot}20PbO{\cdot}xBi_2O_3{\cdot}(50\text{-}x)B_2O_3$ glasses

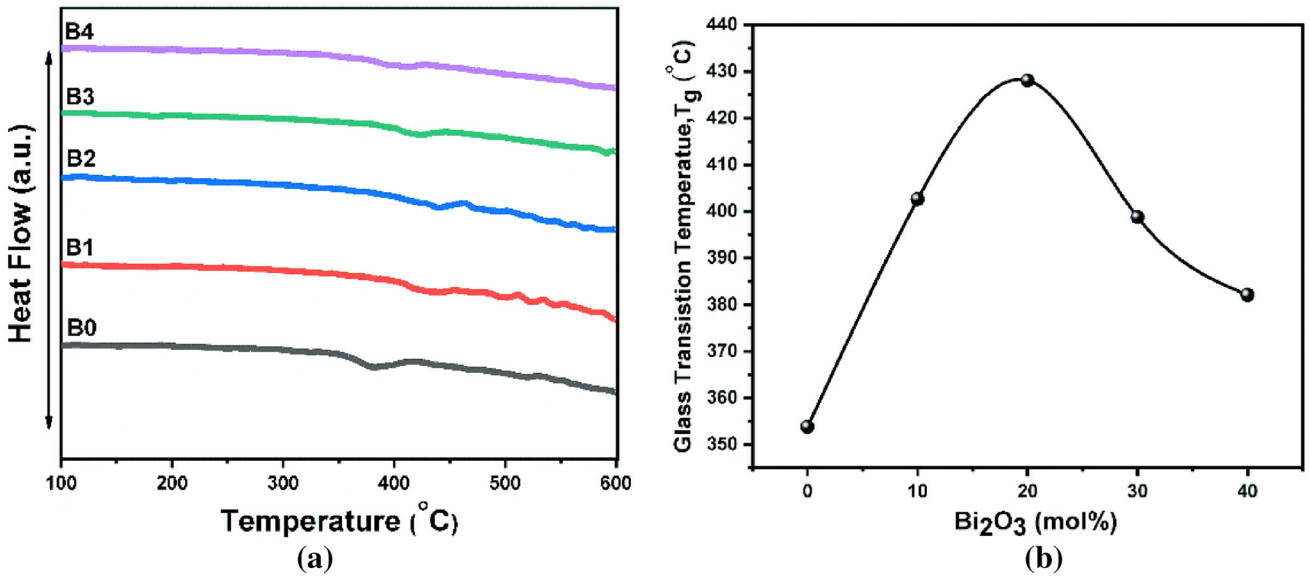

Fig. 3 **a** DSC thermographs for different compositions of $30Li_2O{\cdot}20PbO{\cdot}xBi_2O_3{\cdot}(50\text{-}x)B_2O_3$ glasses. **b** Compositional variation of glass transition temperature with bismuth content for $30Li_2O{\cdot}20PbO{\cdot}xBi_2O_3{\cdot}(50\text{-}x)B_2O_3$glasses

packing density (OPD) is evaluated based on the system density and composition. The values of oxygen molar volume and OPD for each glass sample are presented in Table 1 and variation with bismuth concentration is shown in Fig. 4.

$$OPD = 1000C\left(\frac{D}{M}\right), \tag{4}$$

where C denotes the number of oxygens in the formula unit. We conclude that increasing bismuth concentration in all compositions increases the oxygen molar volume; however, the oxygen packing density decreases. The observed rise in oxygen molar volume and decrease in OPD implies an increase in non-bridging oxygen contribution with the addition of bismuth to the glass matrix. This kind of behavior has also been observed in $Li_2O.Bi_2O_3.B_2O_3.V_2O_5$ glasses [24]. The concentrations of bismuth ions in prepared samples are calculated by using Eq. (5):

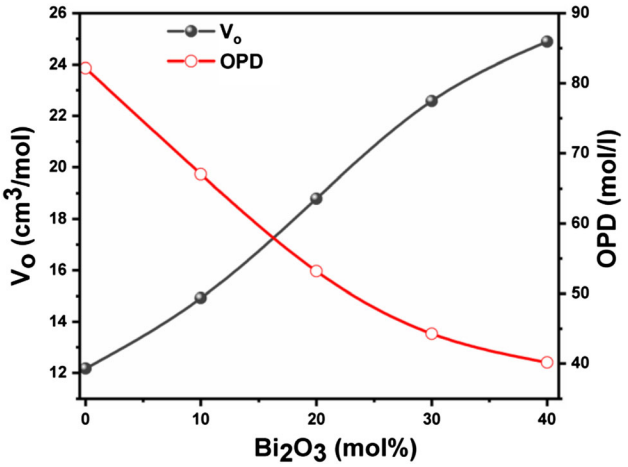

Fig. 4 Variation of oxygen molar volume and oxygen packing density with bismuth content for 30 Li_2O·20PbO·xBi_2O_3·(50-x)B_2O_3glasses

$$N\left(\frac{ions}{cm^3}\right) = \frac{(Avogadro's\ number) \times (glass\ denisty) \times (mol\%\ of\ ions)}{(Average\ molecular\ weight)}. \quad (5)$$

From Table 1, it was found that the ionic concentration of Bi^{3+} ions is increased in the order of 10^{21} cubic centimeters. The polaron radius (r_p) and interionic radii (r_i) were calculated by using the standard formula in Eqs. (6) and (7), in which N represents the ionic concentration [32]:

$$r_p = \frac{1}{2}\left[\frac{\pi}{6N}\right]^{1/3}, \quad (6)$$

$$r_i = \left[\frac{1}{N}\right]^{1/3}. \quad (7)$$

The increased concentration of Bi^{3+} ions in the glass matrix reduced the polaron and interionic radii due to decreasing the distorted lattice site. Similar orders in N, $r_{p,}$ and r_i in have also been reported by Subhadra et al. [24] and Stalin et al. [23] in lithium bismuth borate glasses. The field strength (F) of the samples was calculated by the given equation [32]:

$$F = \left(\frac{Z}{r_p^2}\right). \quad (8)$$

With the addition of the Bi^{3+} ion attractive forces between ions and adjacent structural units increase, increasing the field strengths with a decrease in the interionic distance.

3.2 FTIR spectroscopy studies

Figure 5 depicts the active FTIR region for present glasses characterized by several broad peaks in the range 400–2000 cm^{-1}, known as the fingerprint region. Deconvoluted spectra are shown in Fig. 6a–e and Table 2 lists the compilation of the data of deconvoluted spectra, providing peak position (X_C), amplitude (A), and full width of half maxima (W) of the peaks. From past studies, it is well known that the FTIR spectrum of borate glasses is classified into three broad regions [34–36] that are shown in Fig. 5. The first region from 650–800 cm^{-1}, is ascribed to bending of B-O-B linkages in BO_3 triangles. Another region lies in the range of 800–1150 cm^{-1}, representing the (BO_4) sp^3 tetrahedral unit in stretching vibration of borate. The last region ranging from 1150–1500 cm^{-1} shows the (BO_3) sp^2 planar unit in the B-O and B-O^- stretching vibration of BO_3 and BO_2O^- unit [37]. In the present samples, one more absorption region is observed in the range of 400–600 cm^{-1} associated with the different types of metallic vibration. The location near band 450 cm^{-1} may be due to the rattling motion of lithium ions in their local site [38]. A highly distorted BiO_6 unit shows a band around ~ 472 cm^{-1} due to the Bi-O bonds vibration [39]. This region also shows the presence of symmetrical bending vibration of the PbO_4 tetrahedral structural unit [40]. The low-intensity refined peak at 622 cm^{-1} in the pure sample

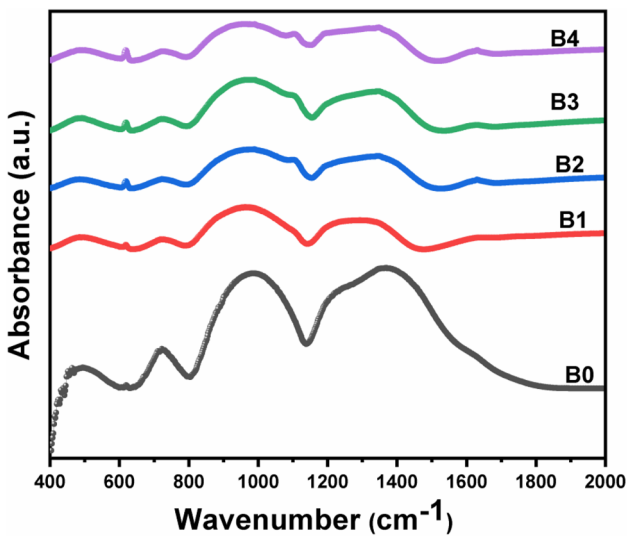

Fig. 5 FTIR spectra of different compositions of 30Li_2O·20PbO·xBi_2O_3·(50-x)B_2O_3 glass system in the spectral range 400–2000 cm^{-1}

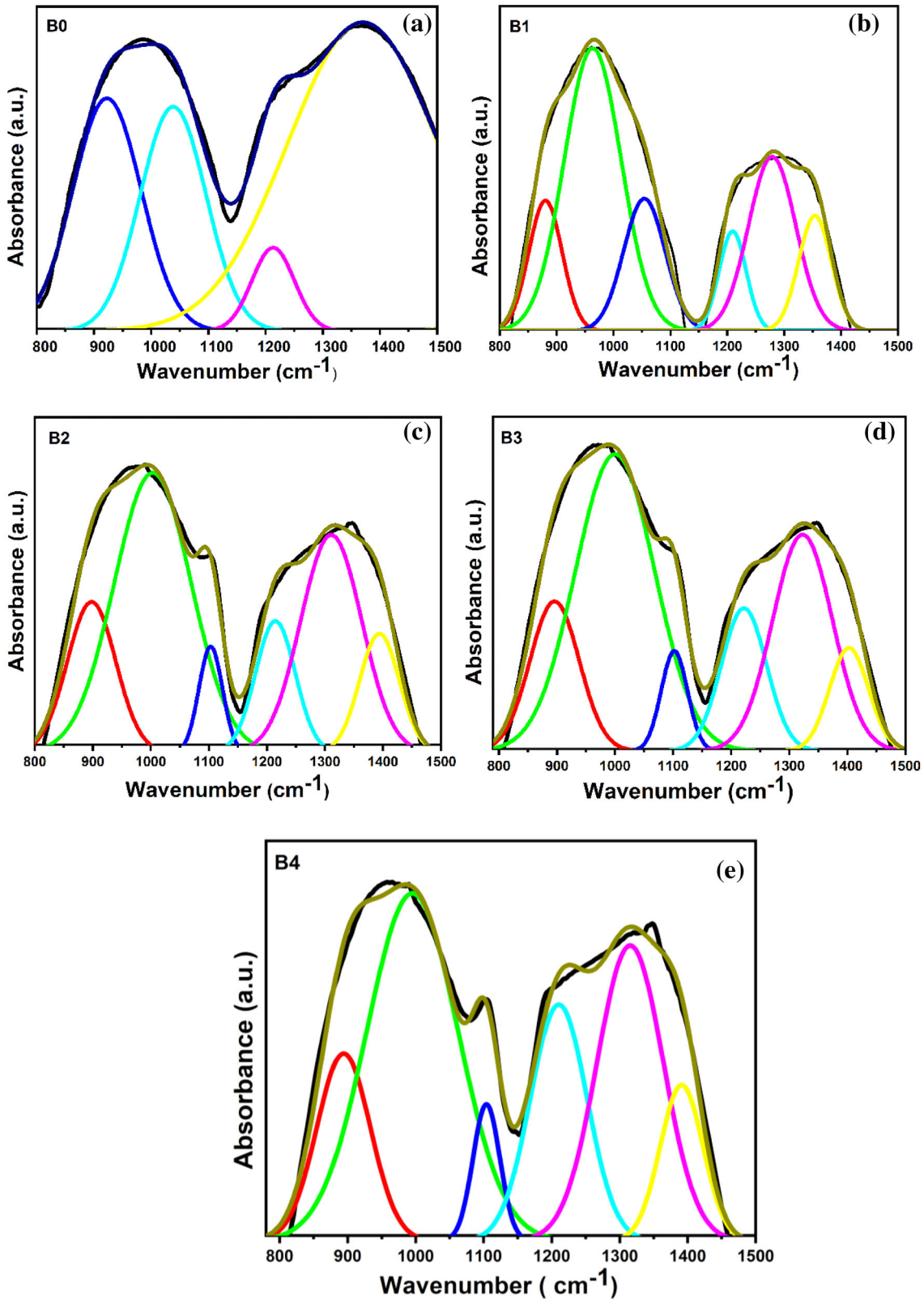

Fig. 6 **a–e** Deconvoluted FTIR spectra of each composition of $30Li_2O{\cdot}20PbO{\cdot}xBi_2O_3{\cdot}(50\text{-}x)B_2O_3$ glass system in the spectral range 800–1500 cm^{-1}

Table 2 Peak position (X_c), amplitude (A), and full width at half maxima (W) of deconvoluted peaks of FTIR spectra of different compositions of $30Li_2O{\cdot}20PbO{\cdot}xBi_2O_3{\cdot}(50\text{-}x)B_2O_3$ glass system

Peak no	x = 0			x = 10			x = 20			x = 30			x = 40		
	X_c (cm^{-1})	A (a.u)	W (cm^{-1})	X_c (cm^{-1})	A (a.u)	W (cm^{-1})	X_c (cm^{-1})	A (a.u)	W (cm^{-1})	X_c (cm^{-1})	A (a.u)	W (cm^{-1})	X_c (cm^{-1})	A (a.u)	W (cm^{-1})
1	–	–	–	880	11	69	897	18	98	896	23	99	894	15	92
2	922	139	141	968	42	117	1003	55	15	1000	76	160	995	50	157
3	1038	128	135	1054	14	86	1103	6	47	1102	8	53	1104	5	46
4	1213	30	87	1209	7	55	1214	13	80	1221	20	91	1210	2	97
5	–	–	–	1278	21	97	1310	34	123	1322	42	121	1315	31	114
6	1370	405	310	1354	10	67	1394	12	81	1402	13	79	1391	10	74

(Fig. 5) is related to the symmetric oscillation of bending B-O-B bond in BO_3 unit. The intensity of the peak is small due to the absence of bismuth in pure sample. As the growth of Bi_2O_3 content increase from $10 \leq x \leq 40$ intensity and size of the peak increase. This is due to the Bi-O bonds vibration at the different wavelengths in distorted BiO_6 polyhedral [27, 41]. For all compositions, the peak found in the band region from 650 to 800 cm^{-1} ascribed to the stretching of B-O-B bond in bending vibrations of BO_3 pentaborate unit. Similar findings were observed by Moustafa et al. [42] and Ali et al. [43] in bismuth borate glass systems. Table 3 provides the assigned vibrational modes for observed infrared bands for all the present glasses. The deconvoluted data region, 800–1150 cm^{-1} (Table 2), exhibits various absorption peaks for different concentrations of bismuth. The band region in wavenumber range from 880–897 cm^{-1} may be attributed to the symmetrical stretching vibration of Bi-O bond in BiO_3 pyramidal units [44, 45]. This band is not present in the pure sample due to the absence of Bi_2O_3. The analysis of peaks found from 922–1003 cm^{-1} shows the peaks at ~ 922, ~ 968, ~ 995, ~ 1000, ~ 1003 cm^{-1} and from 1038–1104 cm^{-1} shows the peaks at ~ 1038, ~ 1054, ~ 1102, ~ 1103, ~ 1104 cm^{-1}, which may be attributed to the B-O bonds stretching vibration in BO_4 unit from a varied-type borate group [46–48]. It can be predicted that bismuth may act as network modifier as well as network former in these compositions. However, the increasing concentration of bismuth oxide resulted in a change in the structure of the BO_3 triangle to BO_4 tetrahedra being near the energy required to break B-O-B bridges and form non-bridging oxygen and formed various types of the structural units [37]. In the same range of spectra,

Table 3 Infrared wavenumber and assignments of vibrational modes of $30Li_2O{\cdot}20PbO{\cdot}xBi_2O_3{\cdot}(50\text{-}x)B_2O_3$ glass system

Wavenumber (cm^{-1})	IR band assignments	References
~ 450	Rattling motion of lithium ions in their local site	[38]
~ 472	Bi-O bonds vibration/PbO_4 tetrahedral structural units	[39, 40]
~ 622	Symmetric oscillations of bending B-O-B bond in BO_3 unit in pure sample/Bi-O bonds vibration at the different wavelengths in distorted BiO_6 polyhedral	[27, 41]
~ 650–800	Bending of B-O-B linkages in BO_3 triangles	[42, 43]
~ 880–897	Symmetrical stretching vibration of Bi-O bond in BiO_3 pyramidal units	[44, 45]
~ 922–1104	B-O bond stretching vibration in BO_4 unit	[46–48]
~ 1209–1278	B-O bond stretching vibration of BO_3 trigonal unit	[50]
~ 1310–1322	B-O bond stretching vibration of various borate groups	[50]
~ 1354–1402	Asymmetrical stretching vibration of borate triangle with BO_3, BO_2O^-, and stretching vibration of borate triangle with (NBO) in various borate group	[51, 52]

Abu-Khadra et al. [49] and Nagaraju et al. [22] have also found the similar structural variations for cobalt doped lead borate glasses. Observed band in the region 1150–1500 cm^{-1}centered at 1290 cm^{-1} shows the peaks at ~ 1209, ~ 1210, ~ 1213, ~ 1214, ~ 1221, ~ 1278, ~ 1310, ~ 1315, ~ 1322, ~1354, ~ 1370, and ~ 1391, ~ 1394, ~ 1402 cm^{-1}. Peak found in the region 1209–1278 cm^{-1} may be related to the B-O stretching vibration of the BO_3 trigonal unit. The peaks at ~ 1310, ~ 1315, and ~ 1322 cm^{-1} may be attributed to the B-O bond stretching vibration of various borate groups [50]. Also, peaks visible in the range 1354–1402 cm^{-1} ascribed to asymmetrical stretching vibration of borate triangle with BO_3, BO_2O^- and stretching vibration of borate triangle with (NBO) in various borate groups [51, 52]. Similar bands are observed by Ganguli et al. in the spectra of Li_2O-PbO-B_2O_3 glasses [53]. The band intensity around 1350–1450 cm^{-1} decreased due to the non-bridging oxygen atoms in the glass network [53] which again reinforce the fact of production of BO_4 structural unit at the expense of the BO_3 structural unit. A similar type of behavior has been observed by Cheng et al. [39] and Stone et al. [54] in the binary glass system B_2O_3-Bi_2O_3. A keen observation of deconvoluted spectra shows that the peak intensities at 1150–1500 cm^{-1} progressively increase with an increase in bismuth concentration, indicating a population of NBOs. Intensity and width of the peak in pure sample found maximum at1038 cm^{-1}. Furthermore, when the concentration of bismuth increases from 10 to 40 mol% the width and intensity of the peaks become small and shifted toward higher wavenumber, that indicating more randomness in the network. The distinctive band at 1630 cm^{-1} may be attributed to the bending vibration of H–O–H bond caused by the hygroscopicity of the analyzed glasses in all samples [52]. The deconvolution approach might be utilized to get N_4 for various borate glasses [50] when various oxides have changed. The resulting values were found to be in good agreement (Table 1).

$$N_4 = \frac{A_4}{A_4 + A_3}, \tag{9}$$

where A_4 represents the peak area at 800–1150 cm^{-1} for the BO_4 unit, and A_3 denotes the peak area at 650–800 cm^{-1} and 1150–1500 cm^{-1} corresponding to the BO_3 unit, respectively. It has been observed that the maximum fractional units of borate are present in pure samples which clearly confirmed the absence of bismuth. After that when the concentration of bismuth increases, borate units decrease as compared to pure sample.

3.3 Optical properties

UV–Vis–NIR spectroscopy is the best technique for characterizing the optical properties of glass materials. Optical absorption coefficient (α) was estimated at various wavelengths by using the following relationship [55]:

$$\alpha(v) = \frac{1}{d}\ln\left(\frac{I_0}{I_T}\right), \tag{10}$$

where d is the thickness of the glass sample, I_0 represents the intensity of the incident beam, and I_T is the transmitted beam, respectively. Absorbance is represented by the factor ln (I_o/I_T).

Figure 7 describes the optical transmission spectra recorded for all compositions and forms a red shift in cutoff wavelength (λ_C) with the increase in Bi_2O_3 concentration. In terms of physical properties, an increase in non-bridging oxygen (NBO) atoms is most likely responsible for the increase in molar volume. In the present system, Bi_2O_3 works as a network modifier at moderate concentrations and dilutes into the matrix without breaking the B-O-B bonds. However, at higher concentrations of Bi_2O_3, B-O-B bonds are replaced by Bi-O-B and Bi-O-Bi bonds. This is attributed to the increase in NBO ions in the glass

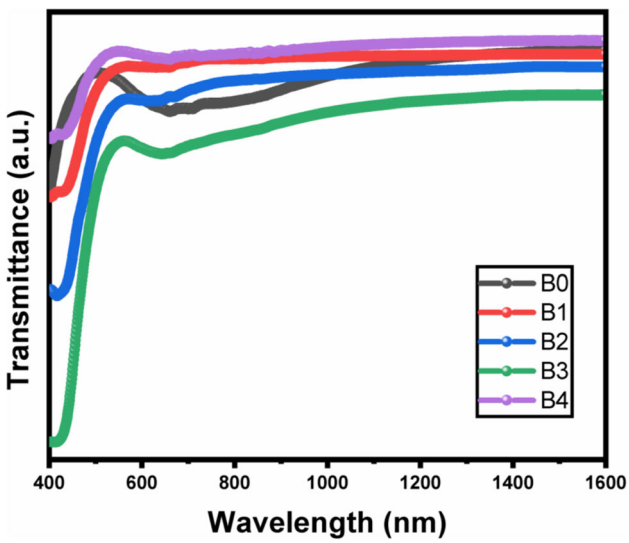

Fig. 7 Optical transmission spectra of $30Li_2O{\cdot}20PbO{\cdot}xBi_2O_3{\cdot}(50\text{-}x)B_2O_3$ glasses

matrix. Also, from Fig. 7, it is clear that these samples have a large transmission region which makes them suitable for IR transmission window [25]. Optical band gap energy was calculated by the relation [55]

$$\alpha(v) = \frac{B\ (h\nu - Eg\ )^n}{h\nu}, \tag{11}$$

where B is the band tailing parameter, E_g is the bandgap energy, and hν is the photon energy. The values of n are determined by the types of optical transitions as indirect allowed, direct allowed, indirect forbidden, and direct forbidden transitions and correspond to n = 2, 1/2, 3, 1/3, respectively. Indirect transitions were established in the prepared series. The absorption edge is divided into three regions. The first region is the high absorption region which is known as the "Tauc Region" as shown in Fig. 8.

From Tauc's plot, the energy band gap is calculated by taking the linear area of the curves toward the energy axis at the $(\alpha h\nu)^{1/2} = 0$ and the values are listed in Table 4. For the present transition band gap energy decreases with increased bismuth concentration, which attributed to the structural changes and increases in NBO ions which is also supported by IR spectra. As Bi^{3+} cation has large polarizing power, which affects the anion charge of O^{2-} ions. The same type of behavior was observed by Mahmoud in lithium bismuth borate glasses [13], Sharma et al. in cadmium-containing sodium borate glasses [55], and Raut et al. in vanadium lithium bismuth borate glasses [56]. The second region appears due to

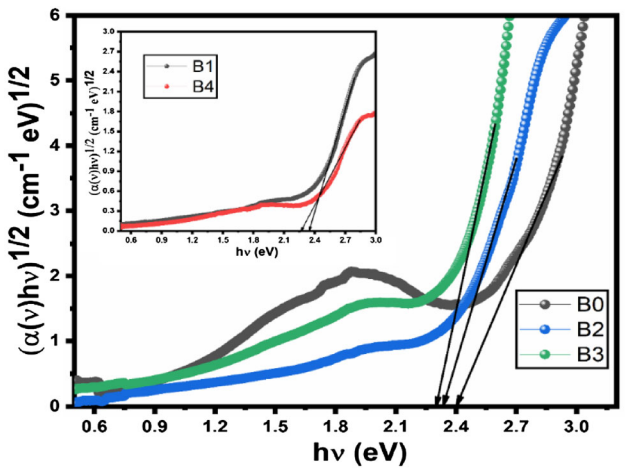

Fig. 8 Tauc's plots for all the samples of $30Li_2O{\cdot}20PbO{\cdot}xBi_2O_3{\cdot}(50\text{-}x)B_2O_3$ glass system for n = 2 (for x = 0 to 40 mol%)

structural disorientation of the materials, known as the "Urbach region". Calculating the slope between ln(α) and hν from the Urbach energy curve (Fig. 9), values of ΔE may be computed by taking the reciprocal. Standard Eq. (12) can also be used to illustrate this relationship

$$\ln \alpha(v) = \frac{h\nu}{\Delta E} + \text{constant}. \tag{12}$$

The minimum value of Urbach's energy (Table 4) at a high concentration of bismuth indicates the possibility of long-range order and minimum defect concentration indicates optical stability is maximum. The decrease in band gap energy is consistent with Urbach's energy which can be explained in terms of a fundamental transformation of present glass samples. By increasing the Bi_2O_3 concentration, the bond length of the BO_3 structural unit rises in direct proportion to the molar volume, resulting in more non-bridging oxygen. These characteristics, together with the lesser bond strength of Bi–O (80.3 kcal/mol) compared to the bond lengths of B–O (192.7 kcal/mol) and Li–O (333.5 kcal/mol), would [13] reduce optical band gap energy and Urbach's energy values. The third region arises due to weak absorption. The refractive index values can be calculated using the following equation [57]:

$$\left(\frac{n^2-1}{n^2+2}\right) = 1 - \sqrt{\frac{E_g}{20}}. \tag{13}$$

In Fig. 10, it is explicitly shown in the graph the value of the refractive index rises. By analyzing the refractive index, it was observed that non-bridged oxygen ions produce more ionic bond resulting polarization of glass system so that refractive index increases. Similarly, opposite variation observed for E_g is depicted in Fig. 10. This may also be attributed due to the quantum size effect that affects the structure of the band and reduces their energy.

$$R_m = \left(\frac{n^2-1}{n^2+2}\right) V_m, \tag{14}$$

where the R_m is known as the molar refractivity and the value of $\left(\frac{V_m}{R_m}\right)$ is called reflection loss (R_L) [58]. The value of R_m increases and reflection loss decreases with an increase in the concentration of bismuth oxide. The Lorentz–Lorentz notation shows that the molar refractivity of the glass specimen material follows a linearly proportionate relationship

Table 4 Cutoff wavelength (λ_C), optical band gap (E_g), band tailing parameter (B), Urbachs energy (ΔE), refractive index (n), molar refractivity (R_m), reflection loss (R_L), molar polarizability (α_m), metallization criterion (M), oxide ion polarizability (α_o^{2-}), optical basicity (Λ), electronegativity (χ), electronic susceptibility ($_e$), and theoretical optical basicity (Λ_{th}) of $30Li_2O{\cdot}20PbO{\cdot}xBi_2O_3{\cdot}(50\text{-}x)B_2O_3$ glasses

Parameter	B0	B1	B2	B3	B4
λ_C (nm)	447.89	507.39	523.14	537.39	559.38
E_g(eV) $n = 2$	2.40	2.36	2.33	2.30	2.25
B $(cm.eV)^{-1/2}$	6.65	1.49	8.92	8.01	1.59
ΔE (eV)	0.81	0.76	0.75	0.71	0.69
n	2.577	2.592	2.602	2.612	2.632
$R_m(cm^3/mol)$	15.89	19.57	24.73	29.80	33.05
R_L	1.532	1.525	1.520	1.515	1.506
$\alpha_m(Å^3)$	6.30	7.76	9.80	11.81	13.10
M	0.347	0.344	0.342	0.340	0.336
$\alpha_{O^{2-}}$ $(Å^3)$	1.51	1.68	1.91	2.19	2.49
$\Lambda(E_g)$	0.56	0.68	0.79	0.90	0.99
χ	1.00	1.16	1.30	1.45	1.57
χ_e	0.449	0.455	0.459	0.463	0.472
Λ_{th}	0.63	0.71	0.79	0.87	0.95

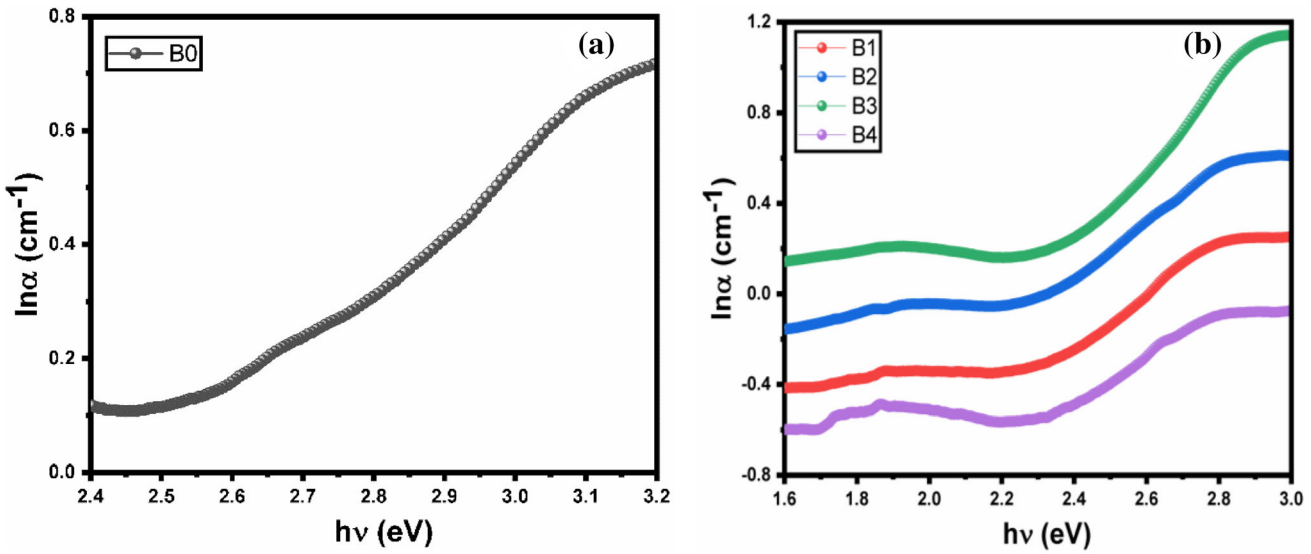

Fig. 9 Urbach's plots for all the samples of $30Li_2O{\cdot}20PbO{\cdot}xBi_2O_3{\cdot}(50\text{-}x)B_2O_3$ glass system **a** for x = 0 **b** x = 10 to 40 mol%

with the molar polarizability (α_m) as shown in Eq. (15) [58]:

$$\alpha_m = \left(\frac{3}{4\pi N_A}\right) R_m, \tag{15}$$

where N_A is Avogadro's number, which denotes the number of electrons associated with an applied electrical field. With varying bismuth concentrations, both molar refractivity as well as molar polarizability follow the same pattern, as shown in Table 4 and depicted in Fig. 11 graphically.

As presented in Eq. (16), the Metallization criterion (M) can be applied to extract information about the material:

$$M = 1 - \frac{R_m}{V_m}. \tag{16}$$

$R_m/V_m < 1$ (non-metallic) and $R_m/V_m \geq 1$ (metallic) are the criteria for identifying the nature of solids according to metallization theory of Herzfeld [59]. The addition of bismuth to the samples results in a significant decrease in the values of the metallization criterion. The expansion impact of both the valence and conduction bands, resulting in a narrow bandgap, is responsible for this pattern. These metallization criterion results are consistent with the reported optical band gap energy measurements. The oxide ion polarizability ($\alpha_{O^{2-}}$) established by band

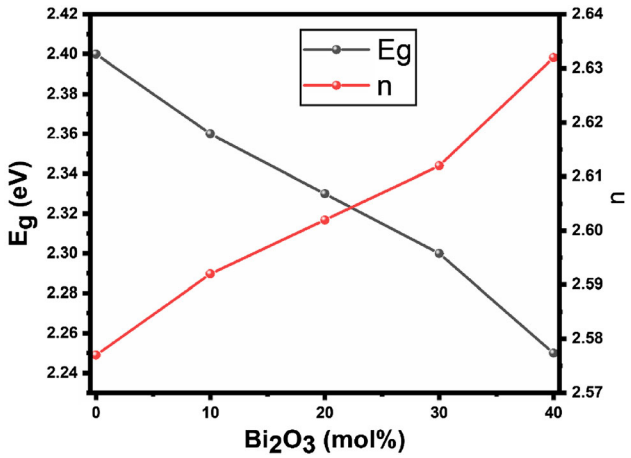

Fig. 10 Variation of refractive index and band gap energy with Bi_2O_3 concentration for all the compositions of $30Li_2O{\cdot}20PbO{\cdot}xBi_2O_3{\cdot}(50\text{-}x)B_2O_3$ glasses

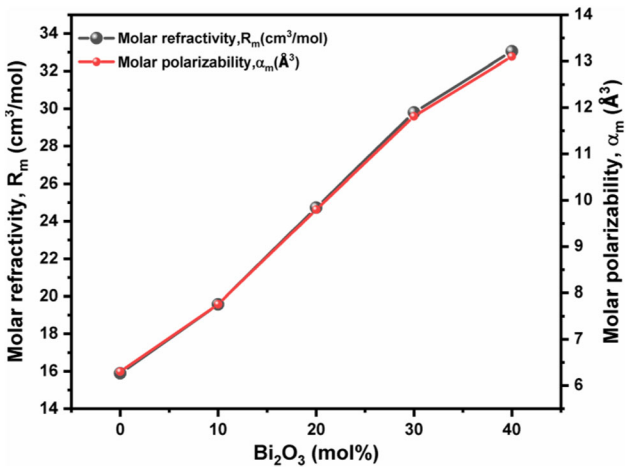

Fig. 11 Dependence of molar refractivity values and electronic polarizability with Bi_2O_3 concentration for all the compositions of $30Li_2O{\cdot}20PbO{\cdot}xBi_2O_3{\cdot}(50\text{-}x)B_2O_3$ glasses

gap energy can be attributed from optical absorption data by using mathematical relation (17) [60, 61].

$$\alpha_{O^{2-}} = \left[\frac{V_m}{2.52}\left(1-\sqrt{\frac{E_g}{20}}\right)-\sum_i p\alpha_i\right]q^{-1}, \tag{17}$$

where α_i is the cation polarizability, p signifies the number of cations, and q stand for number of oxide ion, respectively, in the chemical formula A_pO_q. The computed oxide ion polarizability is found to be increased with increase in the concentration of bismuth oxide (Table 4). Since Bi^{3+} ions have high polarizability, the lone pair bond pair repulsion is greater than bond pair bond pair repulsion. A similar pattern is observed in optical basicity (Λ) calculated by the relations

$$\Lambda = 1.67\left(1-\frac{1}{\alpha_{O^{2-}}}\right), \tag{18}$$

$$\chi = \frac{\Lambda}{0.75}+0.25, \tag{19}$$

$$\chi_e = \frac{(n^2-1)}{4\pi}. \tag{20}$$

Electronegativity is a characteristic of oxide glasses that indicates how powerfully an ion can bind electrons. As result in the data given in Table 4, the value of electronegativity of the ions is greater, the ions will attract more strongly toward the associated oxide ions, resulting in strong bonding between ion networks. Dimitrov, Sakka [60, 62], and Komatsu [60] discovered advantageous relationships between oxide ions electronegativity, cation polarizability, and optical basicity. By considering those relations it has been discovered that glasses with enhanced bismuth oxide content may vary their electronegativity (as shown in Fig. 12).

The covalent and ionic nature of bonding of Lewis acid–base gives results of optical basicity. Electronic polarizability and electronegativity are the parameters that are interlinked with this [63]. By assigning basicity values to certain oxides, it is feasible to establish a "theoretical" optical basicity value, Λ_{th}, for any oxide substance that has been computed using the following equation:

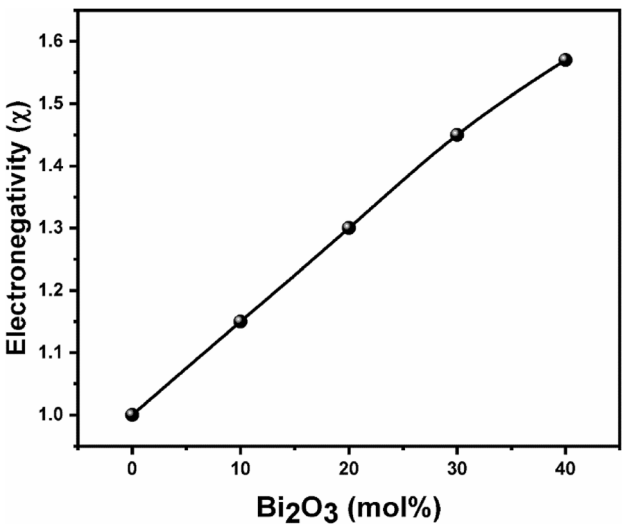

Fig. 12 Variation of electronegativity of $30Li_2O{\cdot}20PbO{\cdot}xBi_2O_3{\cdot}(50\text{-}x)B_2O_3$ glasses with Bi_2O_3 concentration

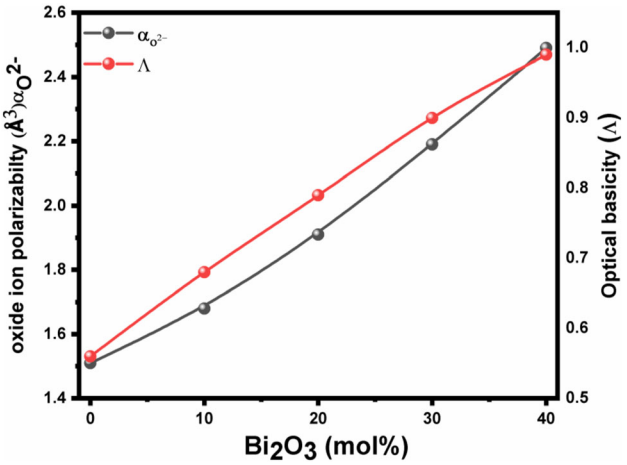

Fig. 13 Plots of oxide ion polarizability and optical basicity of $30Li_2O{\cdot}20PbO{\cdot}xBi_2O_3{\cdot}(50\text{-}x)B_2O_3$ glasses with Bi_2O_3 concentration

$$\Lambda_{th} = \Lambda_{Li_2O}.X_{Li_2O} + \Lambda_{PbO}.X_{PbO} + \Lambda_{Bi_2O_3}.X_{Bi_2O_3} + \Lambda_{B_2O_3}.X_{B_2O_3}, \quad (21)$$

where $X_{Li_2O}, X_{PbO}, X_{Bi_2O_3}, X_{B_2O_3}$ denotes the molar percentage of oxides of glass samples and $\Lambda_{Li_2O}, \Lambda_{PbO}, \Lambda_{Bi_2O_3}, \Lambda_{B_2O_3}$ denotes the optical basicity of oxides as calculated by References [60].

An increase in optical basicity specifies the higher ability of electron transfer between oxide ions and cation. It is also feasible to determine what kinds of bonds are present in the glass system. A high value of optical basicity indicates more significant ionic interaction, whereas a low value indicates covalent bonding [64]. The increase in Λ is presented in Fig. 13 suggest that the ionic character of the analyzed glass system increases with Bi_2O_3 content and is supported by FTIR and absorption spectra results.

4 Conclusions

A new glass series having composition $30Li_2O{\cdot}20PbO{\cdot}xBi_2O_3{\cdot}(50\text{-}x)B_2O_3$; (where x = 0 to 40 mol%) was synthesized by the conventional melt quenching method and their various structural properties were obtained to know the influence of conditional glass former Bi_2O_3 on the host glass structure. The presence of broad haloes ~ 28° confirms the short-range order ascertained amorphous nature of glass samples. Different physical parameters, such as density, molar volume, crystalline volume, and OPD values, were also observed. Density and molar volume of these samples found to be increased from 3.63 to 4.96 g/cm^3 and from 24.35 to 49.78 cm^3/mol, respectively, with concentration of bismuth. On increasing the bismuth oxide, the structural units BO_3 transformed into BO_4 structural units obtained from the FTIR analysis. The band 880–897 cm^{-1} in wavenumber region attributed to the symmetrical stretching vibration of Bi-O bond in BiO_3 pyramidal units. Also, the band intensity around the band region 1350–1450 cm^{-1} decreased which reveals that NBO's increased in the glass matrix at the expense of Bi_2O_3 content. From the optical analysis, the various parameters were also examined. The indirect allowed optical transition is feasible. Cutoff wavelength increases from 447 to 559 nm and bandgap energy decreases from 2.40 to 2.25 eV due to the influences of bismuth content that affect the NBO's ion and reduce the bandgap energy. An overall analysis of these results suggest the suitability of the present glasses in the area of photonics, such as for infrared transmitting materials and nonlinear optical systems.

Author contributions

SC contributed to conceptualization, methodology, data curation, and writing of the original draft. RB contributed to supervision, methodology, and writing, reviewing & editing of the manuscript. SG performed reviewing and editing of the manuscript. SR contributed to data curation, reviewing, and editing of the manuscript.

Funding

The authors have not disclosed any funding.

Data availability

All the data analyzed in this work are included in this article.

Declarations

Conflict of interest The authors declare that they have no known competing financial interests or

personal relationships that could have appeared to influence the work reported in this paper.

Ethical approval The contents of our research paper "Effect of Bi_2O_3 on structural and optical properties of $Li_2O{\cdot}PbO{\cdot}Bi_2O_3{\cdot}B_2O_3$ glasses" are new and we have synthesized these samples for the first time using melt quenching technique. It is certified that the work is completely original and has not been published/ submitted for publication elsewhere. We will follow all the norms of the publication, like copyrights, etc.

References

1. J. Dahiya, A. Hooda, A. Agarwal, S. Khasa, Tuneable colour flexibility in Dy^{3+} & Eu^{3+} co-doped lithium fluoride bismuth borate glass system for solid state lighting applications. J. Non-Cryst. Solids **576**, 121237 (2022). https://doi.org/10.1016/j.jnoncrysol.2021.121237
2. M. Bengisu, Borate glasses for scientific and industrial applications: a review. J. Mater. Sci. **51**(5), 2199–2242 (2016). https://doi.org/10.1007/s10853-015-9537-4
3. P. Yasaka, N. Pattanaboonmee, H.J. Kim, P. Limkitjaroenporn, J. Kaewkhao, Gamma radiation shielding and optical properties measurements of zinc bismuth borate glasses. Ann. Nucl. Energy **68**, 4–9 (2014). https://doi.org/10.1016/j.anucene.2013.12.015
4. I. Kashif, A. Abd El-Maboud, A. Ratep, Effect of Nd_2O_3 addition on structure and characterization of lead bismuth borate glass. Results. Phys. **4**, 1–5 (2014). https://doi.org/10.1016/j.rinp.2013.11.002
5. S.D. Kamath, A. Wagh, M.P. Ajithkumar, Composition dependent structural and thermal properties of SM_2O_3 Doped zinc fluoroborate glasses. Energy Res. J. **4**(2), 52–58 (2013). https://doi.org/10.3844/erjsp.2013.52.58
6. N. Deopa, A.S. Rao, Spectroscopic studies of Sm^{3+} ions activated lithium lead alumino borate glasses for visible luminescent device applications. Opt. Mater **72**, 31–39 (2017). https://doi.org/10.1016/j.optmat.2017.04.067
7. M. Purnima, S. Stalin, A. Edukondalu, M.A. Samee, S.K. Ahmmad, S. Rahman, Spectroscopic studies on Li_2O–MgO–Bi_2O_3–B_2O_3 glasses. Chin. J. Phys. **66**, 517–526 (2020). https://doi.org/10.1016/j.cjph.2020.05.031
8. Sanjay, N. Kishore, A. Agarwal, I. Pal, S. Devi, R. Bala, Characterization and optical properties of MoO_3-PbO-B_2O_3 semiconducting glasses. AIP Conf. Proceedings **1942**, 140012 (2018). https://doi.org/10.1063/1.5029143
9. A.I. Ismail, A. Samir, F. Ahmad, L.I. Soliman, A. Abdelghany, Spectroscopic studies and the effect of radiation of alkali borate glasses containing chromium ions. J. Non-Cryst. Solids **565**, 120743 (2021). https://doi.org/10.1016/j.jnoncrysol.2021.120743
10. N.N. Ahlawat, P. Aghmkar, N. Ahlawat, A. Agarwal, Monica, Rekha, structural study of TM doped alkali bismuth borate glasses. Adv. Mat. Lett. **4**(1), 71–73 (2013). https://doi.org/10.5185/amlett.2013.icnano.252
11. S.M. Kamil, A.A. Abul-Magd, W. El-Gammal, H.A. Saudi, Enhanced optical and structural features of Ni^{2+}/La^{3+} hybrid borate glasses. Spectrochim. Acta A Mol. Biomol. Spectrosc. **267**, 120569 (2022). https://doi.org/10.1016/j.saa.2021.120569
12. M. Kaur, M.S. Saini, Synthesis and characterization of lithium borate glasses containing bismuth. Int. J. Adv. Res. Phys. Sci. **1**(8), 1–8 (2014)
13. K.H. Mahmoud, Optical study of lithium–bismuth–borate glasses. Int. J. Appl. Ceram. Technol. **6**(2), 279–285 (2009). https://doi.org/10.1111/j.1744-7402.2008.02268.x
14. A.F. Wells, *Structural inorganic chemistry*, 4th edn. (Clarendon Press, Oxford, 1975)
15. H. Masai, Y. Takahashi, T. Fujiwara, T. Suzuki, Y. Ohishi, Correlation between near infrared emission and bismuth radical species of Bi_2O_3-containing aluminoborate glass. J. Appl. Phys. **106**, 103523 (2009). https://doi.org/10.1063/1.3264631
16. R. Bala, A. Agarwal, S. Sanghi, N. Singh, Effect of Bi2O3 on nonlinear optical properties of ZnO.Bi2O3.SiO2 glasses. Opt. Mater. **36**, 352–356 (2013). https://doi.org/10.1016/j.opmat.2013.09.021
17. K. Terashima, T. Shimoto, T. Yoko, Structure and nonlinear optical properties of PbO-Bi_2O_3-B_2O_3 glasses. Phys. Chem. Glas. **38**, 211–217 (1997)
18. I.L. Opera, H. Hesse, K. Betzler, Optical properties of Bismuth borate glasses. Opt. Mater. **26**(3), 235–237 (2004). https://doi.org/10.1016/j.optmat.2003.10.006
19. I. Agarwal, S. Pal, M.P. Sanghi, Agarwal, Judd-Ofelt parameters and radiative properties of Sm^{3+} ions doped zinc bismuth borate glasses. Opt. mater. **32**(2), 339–344 (2009). https://doi.org/10.1016/j.optmat.2009.08.012
20. M.I. Sayyed, S.A.M. Issa, H.O. Tekin, Y.B. Saddeek, Comparative study of gamma-ray shielding and elastic properties of BaO–Bi_2O_3–B_2O_3 and ZnO–Bi_2O_3–B_2O_3 glass systems. Mater. Chem. Phys. **217**, 11–22 (2018). https://doi.org/10.1016/j.matchemphys.2018.06.034
21. A. Kumar, Gamma-ray shielding properties of PbO-Li_2O-B_2O_3 glasses. Radiat. Phys. Chem. **136**, 50–53 (2017). https://doi.org/10.1016/j.radphyschem.2017.03.023
22. R. Nagaraju, B. Devaiah, L. Haritha, K.C. Sekhar, Md. Shareefuddin, M.A. Sayed, G. Lalitha, K.V. Kumar, Influence

of CaF_2 on spectroscopic studies of lead fluoro bismuth borate glasses doped with Cr^{3+} ions. J. Non-Cryst. Solids **560**, 120705 (2021). https://doi.org/10.1016/j.jnoncrysol.2021.120705

23. S. Stalin, D.K. Gaikwad, M.S. Al-Buriahi, C. Srinivasu, S.A. Ahmmad, H.O. Tekin, S. Rahman, Influence of Bi_2O_3/WO_3 substitution on the optical, mechanical, chemical durability and gamma ray shielding properties of lithium-borate glasses. Ceram. Int. **47**(4), 5286–5299 (2020). https://doi.org/10.1016/j.ceramint.2020.10.109
24. M. Subhadra, S. Sulochana, P. Kistaiah, Effect of V_2O_5 content on physical and optical properties of lithium bismuth borate glasses. Mater. Today: Proc. **5**, 26417–26423 (2018). https://doi.org/10.1016/j.matpr.2018.08.095
25. S. Rani, S. Sanghi, N. Ahlawat, A. Agarwal, Influence of Bi_2O_3 on thermal, structural and dielectric properties of lithium zinc bismuth borate glasses. J. Alloys Compd. **597**, 110–118 (2014). https://doi.org/10.1016/j.jallcom.2014.01.211
26. E.M. Abou Hussein, T.D. Abd Elaziz, N.A. El-Alaily, Effect of gamma radiation on some optical and electrical properties of lithium bismuth silicate glasses. J Mater Sci: Mater Electron **30**, 12054–12064 (2019). https://doi.org/10.1007/s10854-019-01563-y
27. J. Bhemarajam, P. SyamPrasad, M. MohanBabu, M. Özcan, M. Prasad, Investigations on structural and optical properties of various modifier oxides (MO = ZnO, CdO, BaO, and PbO) containing bismuth borate lithium glasses. J. Compos. Sci. **5**(12), 308 (2021). https://doi.org/10.3390/jcs5120308
28. H.D. Prakash, S. Mahamuda, J.S. Alzahranii, P. Sailaja, K. Swapna, M. Venkateswarlu, A.S. Rao, Z.A. Alrowaili, I.O. Olarinoye, M.S. Al-Buriahi, Synthesis and characterization of B_2O_3-Bi_2O_3-SrO-Al_2O_3-PbO-Dy_2O_3 glass system: The role of Bi_2O_3/Dy_2O_3 on the optical, structural, and radiation absorption parameters. Mat. Res. Bull. **155**, 111952 (2022). https://doi.org/10.1016/j.materresbull.2022.111952
29. K.M. Katubi, I.O. Olarinoye, Z.A. Alrowaili, M.S. Al-Buriahi, Optical transmission, polarizability, and photon/neutron shielding properties of Bi_2O_3/MnO/B_2O_3 glass system. Optik **268**, 169695 (2022). https://doi.org/10.1016/j.ijleo.2022.169695
30. M.A. Alothman, A.M. Al-Baradi, S.B. Ahmed, R. Kurtullus, I.O. Olarinoye, T. Kavas, M.S. Al-Buriahi, Physical, optical, and ionizing radiation shielding parameters of $Al(PO_3)_3$-doped PbO-Bi_2O_3-B_2O_3 glass system. J Mater Sci: Mater Electron **32**, 27744–27761 (2021). https://doi.org/10.1007/s10854-021-07157-x
31. S. Chauhan, R. Bala, S. Rani, S. Gaur, Investigation of structural and optical properties of lithium lead bismuth silicate glasses. J. Mater Sci: Mater Electron **33**(15), 12371–12383 (2022). https://doi.org/10.1007/s10854-022-08194-w
32. R. Kaur, R.B. Rakesh, S.G. Mhatre, V. Bhatia, D. Kumar, H. Singh, S.P. Singh, A. Kumar, Physical, optical, structural and thermoluminescence behaviour of borosilicate glasses doped with trivalent neodymium ions. Opt. Mat. **17**, 111109 (2021). https://doi.org/10.1016/j.optmat.2021.111109
33. S. Thakur, V. Thakur, A. Kaur, L. Singh, Structural, optical and thermal properties of nickel doped bismuth borate glasses. J. Non-Crys. Solids **512**, 60–71 (2019). https://doi.org/10.1016/j.jnoncrysol.2019.02.012
34. A. Yadav, M.S. Dahiya, A. Hooda, P. Chand, S. Khasa, Structural influence of mixed transition metal ions on lithium bismuth borate glasses. Solid State Sci. **70**, 54–56 (2017). https://doi.org/10.1016/j.solidstatesciences.2017.06.011
35. Y.B. Saddeek, E.R. Shaaban, S. El-Moustafa, H.M. Moustafa, Spectroscopic properties, electronic polarizability, and optical basicity of Bi_2O_3–Li_2O–B_2O_3 glasses. Phys. B Condens. Matter. **403**, 2399–2407 (2008). https://doi.org/10.1016/j.physb.2007.12.027
36. M.S. Gaafar, S.Y. Marzouk, H.A. Zayed, L.I. Soliman, A.H. Serag El-Deen, Structural studies and mechanical properties of some borate glasses doped with different alkali and cobalt oxides. Curr. Appl. Phys. **13**(1), 152–158 (2013). https://doi.org/10.1016/j.cap.2012.07.007
37. P. Pascuta, L. Pop, S. Rada, M. Bosca, E. Culea, The local structure of bismuth borate glasses doped with europium ions evidenced by FT-IR spectroscopy. J Mater Sci: Mater Electron **19**, 424–428 (2008). https://doi.org/10.1007/s10854-007-9359-5
38. A.A. Soliman, E.M. Sakr, I. Kashif, The investigation of the influence of lead oxide on the formation and on the structure of lithium diborate glasses. Mater. Sci. Eng. B. **158**(1–3), 30–34 (2009). https://doi.org/10.1016/j.mseb.2008.12.034
39. Y. Cheng, H. Xiao, W. Guo, W. Guo, Structure and crystallization kinetics of Bi_2O_3–B_2O_3 glasses. Thermochim. Acta. **444**(2), 173–178 (2006). https://doi.org/10.1016/j.tca.2006.03.016
40. R.A. Elsad, A.M. Abdel-Aziz, E.M. Ahmed, Y.S. Rammah, F.I. El-Agawany, M.S. Shams, FT-IR, ultrasonic and dielectric characteristics of neodymium (III)/ erbium (III) lead-borate glasses: experimental studies. J Mater. Res. Technol. **13**, 1363–1373 (2021). https://doi.org/10.1016/j.jmrt.2021.05.029
41. M.A. Girsova, S.V. Firstov, T.V. Antropova, Structural and optical properties of the bismuth-containing quartz-like glasses. J. Phys: Conf. Ser. **541**, 012022 (2014). https://doi.org/10.1088/1742-6596/541/1/012022
42. S. El-Moustafa, Y.B. Saddeek, E.R. Shaaban, Structural and optical properties of lithium borobismuthate glasses. J. Phys. Chem. Solids. **69**, 2281–2287 (2008). https://doi.org/10.1016/j.jpcs.2008.04.020

43. A.A. Ali, Y.S. Rammah, R. El-Mallawany, D. Souri, FTIR and UV spectra of pentaternary borate glasses. Meas. J. Int. Meas. Confed. **105**, 72–77 (2017). https://doi.org/10.1016/j.measurement.2017.04.010
44. S. Sanghi, S. Duhan, A. Agarwal, P. Aghamakar, Study of structure and optical properties of $Fe_2O3{\cdot}CaO{\cdot}Bi_2O_3$ glasses. J. Alloys Compd. **488**(1), 454–458 (2009). https://doi.org/10.1016/j.jallcom.2009.09.009
45. G. Gao, L. Hu, H. Fan, G. Wang, K. Li, S. Feng, S. Fan, H. Chen, Effect of Bi_2O_3 on physical, optical and structural properties of boron silicon bismuthate glasses. Opt. Mater. **32**(1), 159–163 (2009). https://doi.org/10.1016/j.optmat.2009.07.005
46. H. Feng, Z. Yuanyuan, X. Junlin, IR and Raman spectra properties of Bi_2O_3-ZnO-B_2O_3-BaO quaternion glass system. Prime Arch Chem **5**, 1142–1150 (2020). https://doi.org/10.4236/ajac.2014.516121
47. S.M. Abo-Naf, F.H. El-Batal, M.A. Azooz, Characterization of some glasses in the system SiO_2, $Na_2O{\cdot}RO$ by infrared spectroscopy. Mater. Chem. Phys. **77**(3), 846–852 (2003). https://doi.org/10.1016/S0254-0584(02)00215-8
48. A. Kumar, S.B. Rai, D.K. Rai, Effect of thermal neutron irradiation on Gd^{3+} ions doped in oxy fluoro borate glass: an infra-red study. Mater. Res. Bull. **38**, 333–339 (2003). https://doi.org/10.1016/S0025-5408(02)01003-6
49. A.S. Abu-Khadra, A.M. Taha, A.M. Abdel-Ghany, A.A. Abul-Magd, Effect of silver iodide (AgI) on structural and optical properties of cobalt doped lead-borate glasses. Ceram. Int. **47**(18), 26271–26279 (2021). https://doi.org/10.1016/j.ceramint.2021.06.036
50. K.S. Shaaban, E.A. AbdelWahab, E.R. Shaaban, E.S. Yousef, S.A. Mahmoud, Electronic polarizability, optical basicity, thermal, mechanical and optical investigations of ($65B_2O_3$–$30Li_2O$–$5Al_2O_3$) glasses doped with titanate. J. Elect. Mater. **49**, 2040–2049 (2020). https://doi.org/10.1007/s11664-019-07889-x
51. N. Elkhoshkhany, N. Samir, E.S. Yousef, Structural, thermal and optical properties of oxy-fluoro borotellurite glasses. J. Mater. Res. Technol. **9**(3), 2946–2959 (2020). https://doi.org/10.1016/j.jmrt.2020.01.045
52. L. Balachander, G. Ramadevudu, M. Shareefuddin, R. Sayanna, Y.C. Veenudhar, IR analysis of borate glasses containing three alkali oxides. Sci. Asia. **39**, 278–283 (2013). https://doi.org/10.2306/scienceasia1513-1874.2013.39.278
53. M. Ganguli, K.J. Rao, Structural role of PbO in Li_2O–PbO–B_2O_3 glasses. J. Solid State Chem. **145**(1), 65–76 (1999). https://doi.org/10.1006/jssc.1999.8221
54. C.E. Stone, A.C. Wright, R.N. Sinclair, S.A. Feller, M. Affatigato, D.L. Hogan, N.D. Nelson, C. Vira, Y.B. Dimitriev, E.M. Gattef, D. Ehrt, Structure of bismuth borate glasses. Phys. Chem. Glasses **41**(6), 409–412 (2000)
55. V. Sharma, S.P. Singh, G.S. Mudahar, K.S. Thind, Synthesis and characterization of cadmium containing sodium borate glasses. New J. Glass Ceram. **2**(4), 128–132 (2012). https://doi.org/10.4236/njgc.2012.24022
56. V.D. Raut, A.V. Deshpande, N.S. Satpute, Study on the modification in physical and optical properties of lithium bismuth borate glasses with vanadium oxide addition. Res. Trend. Chal. Phy. Sci. **5**, 140–149 (2021). https://doi.org/10.9734/bpi/rtcps/v5/1928C
57. N. Elkhoshkhany, R. Abbas, R. El-Mallawany, A.J. Fraih, Optical properties of quaternary TeO_2–ZnO–Nb_2O_5–Gd_2O_3 glasses. Ceram. Int. **40**(9), 14477–14481 (2014). https://doi.org/10.1016/j.ceramint.2014.07.006
58. M. Abdel-Baki, F. Abdel-Wahab, A. Radi, F. El-Diasty, Factors affecting optical dispersion in borate glass systems. J. Phys. Chem. Solids **68**, 1457–1470 (2007). https://doi.org/10.1016/j.jpcs.2007.03.026
59. K.F. Herzfeld, On atomic properties which make an element a metal. Phys. Rev. J. **29**, 701–705 (1927). https://doi.org/10.1103/PhysRev.29.701
60. V. Dimitrov, T. Komatsu, An interpretation of optical properties of oxides and oxide glasses in terms of the electronic ion polarizability and average single bond strength. J. Univ. Chem. Technol. Metall. **45**(3), 219–250 (2010)
61. S.L. SrinivasaRao, G. Ramadevudu, Md. Shareefuddin, A. Hameed, M.N. Chary, M.L. Rao, Optical properties of alkaline earth borate glasses. Int. J. Eng. Sci. Technol. **4**(4), 25–35 (2012). https://doi.org/10.4314/ijest.v4i4.3
62. V. Dimitrov, S. Sakka, Electronic oxide polarizability and optical basicity of simple oxides. J. Appl. Phys. **79**, 1736 (1996). https://doi.org/10.1063/1.360962
63. J.A. Duffy, A review of optical basicity and its applications to oxidic systems. Geochim. Cosmochim. Acta **57**(16), 3961–3970 (1993). https://doi.org/10.1016/0016-7037(93)90346-X
64. J.A. Duffy, Electronic polarisability and related properties of the oxide ion. Phys. Chem. Glasses **30**, 1–4 (1989)